Defect and Diffusion Forum
ISSN: 1662-9507, Vol. 426, pp 71-78
doi:10.4028/p-4mo61y

Submitted: 2022-09-04
Revised: 2022-11-21
Accepted: 2022-11-25
Online: 2023-06-06

Analysis of Basal Plane Dislocation Motion Induced by P+ Ion Implantation Using Synchrotron X-Ray Topography

Zeyu Chen[1,a*], Yafei Liu[1,b], Hongyu Peng[1,c], Qianyu Cheng[1,d], Shanshan Hu[1,e], Balaji Raghothamachar[1,f], Michael Dudley[1,g], Stephen A. Mancini[2,h], Seung Yup Jang[2,i], and Woongje Sung[2,j]

[1]Department of Materials Science & Chemical Engineering, Stony Brook University, Stony Brook, NY 11794 USA

[2]State University of New York Polytechnic Institute, College of Nanoscale Science and Engineering, Albany NY, 12203, USA

[a]Zeyu.chen@stonybrook.edu, [b]Yafei.liu@stonybrook.edu, [c]Hongyu.peng@stonybrook.edu, [d]Qianyu.cheng@stonybrook.edu, [e]Shanshan.Hu@stonybrook.edu, [f]Balaji.raghothamachar@stonybrook.edu, [g]Michael.dudley@stonybrook.edu, [h]Mancins@sunypoly.edu, [i]Jangs@sunypoly.edu, [j]Sungw1@sunypoly.edu

Keywords: 4H-SiC, Ion Implantation, Annealing, Basal Plane Dislocation, Synchrotron X-ray Topography

Abstract. Multiple PIN diodes with junction termination extension (JTE) were fabricated on 4H-SiC wafers with 10 μm thick epilayers by ion implantation with various dosages of Al ions at room temperature (RT) and high temperature (600 ˚C). The subsequent annealing process was conducted at 1650˚C for 10 minutes to activate the dopant atoms and recover the lattice damages introduced by the implantation. Synchrotron X-ray topography was used to characterize the defects in the devices, and it is observed that basal plane dislocations (BPDs) were generated during the annealing process from the boundaries between the high (P+) and low (P-) doping concentration in devices implanted with relatively high doses at RT. Further, topographs also manifest motion of BPDs due to implantation-induced stresses, where BPDs with opposite sign Burgers vectors move in directions accommodative of nature of stress (tensile/compressive). On the other hand, generation of BPDs due to implantation was not observed in devices implanted either at relatively low dosages at both temperatures or relatively high dosages at high temperature. Measurements of blocking behaviors of devices illustrate that devices with higher densities of process-induced BPDs yield higher leakage currents.

Introduction

Silicon Carbide (SiC) is a promising wide bandgap semiconductor for future power devices since it has a wide bandgap, high breakdown voltage and good thermal stability [1]. In recent years, SiC power devices have been successfully fabricated and applied in power and electrical vehicle industries. During device fabrication, a necessary process is selective area doping to create p-n junctions. Nowadays, the most mature method of performing selective area doping in 4H-SiC epiwafer is ion implantation [2]. However, such implantation processes employing high energy ions can damage the lattice in the epilayers that can subsequently lead to lattice stress/strain, since the accelerated dopant atoms will displace the host Si and C atoms. Ion implantation at high energies with relatively low dose level is found to introduce tensile strains within the implanted 4H-SiC epilayers [3,4]. However, implantation with a higher dose level, of the order of 10^{15} cm^{-2}, lattice stress/strain can possibly trigger the formation and migration of basal plane dislocations (BPDs) during the annealing process, which are known to be detrimental to the performance of the devices [5,6,7]. Implantation processes are typically conducted under room temperature (RT) conditions, but high temperature (HT) implantation can be favorable when the dose level is high [8] since the high temperatures can lead to dynamical annealing effect to mitigate the lattice damage during implantation [9,10].

In this study, the motion of BPDs under stress induced by implantation is evaluated in 1.2 kV-rated 4H-SiC PiN diodes with junction termination extension (JTE). The diodes have been fabricated by implantation with different dose levels and concentration profiles under RT and at 600 ˚C and annealed under identical conditions.

Synchrotron monochromatic beam X-ray topography [11] has been employed to characterize the defects in the devices. This non-destructive technique provides a large field of view and clear contrast of defects at nearly micron resolution. For Burgers vectors analysis of the dislocations, ray tracing simulation was employed [12]. Dopant concentration profiles were simulated by stopping and range of ions in matter (SRIM) [13] for the devices implanted under different conditions.

Experiment

1.2 kV-rated PIN diodes were fabricated on 4˚ off-cut 4H-SiC wafer with 10 μm thick epilayer, where the substrate is heavily doped with 1.5 x 10^{18} cm^{-3} and the epilayer is doped with 8 x $10^{15}$$cm^{-3}$ N atoms. Ion implantations were conducted with Al dopant atoms at dose levels of 1×10^{15} cm^{-2}, 5×10^{15} cm^{-2}, and 9×10^{15} cm^{-2}, and under RT for all dosages and under 600 ˚C (HT) for dose levels of 1×10^{15} cm^{-2} and 5×10^{15} cm^{-2}, so we denote the implantation doses and temperature as “1xRT”, “1xHT”, “5xRT”, “5xHT”, and “9xRT”. In addition to that, a device with a box concentration profile was fabricated with dose level of 5x at RT, denoted as “5x Box RT”. Table I shows the details of the conditions of the implantation and their denotaions.

Table I. Details of the conditions of the implantation and their denotations.

Type of Device	Dose(x10^{15} cm^{-2})	Implant Temp(°C)	Comment	Denotation
PIN diode	1.0	RT		1x RT
PIN diode	1.0	600		1x HT
PIN diode	5.0	RT		5x RT
PIN diode	5.0	600		5x HT
PIN diode	5.0	RT	Box profile	5x Box RT
PIN diode	9.0	RT		9x RT

These 2 mm x 2mm devices fabricated are surrounded by JTE. Fig. 1(a) shows the top and cross-sectional view of one side of the devices, where JTEs were designed with hybrid structure consisting of P+ rings with widths of 4 μm embedded in bulk P- JTE region which in turn are surrounded by a series of P- JTE rings. The hybrid structure can handle a wide dose process margin for the JTE implant and the dose for the JTE was optimized through simulations. Fig.1 (b) shows concentration profiles simulated by SRIM for the P+ regions of devices against the background doping level of the epilayer. Comparing 9x RT, 5x RT and 5x Box RT, 9x RT has higher surface concentration, while 5x Box RT has a higher body concentration. The P+ rings also have the same concentration profile as the active region while the P- regions were implanted with 1x10^{18} cm^{-3} Al ions. Details of the devices are described elsewhere [8]. The implanted wafer was carbon capped prior to activation annealing process at 1650 ˚C. The diodes were then stresssed at current density of 125A/cm^2 for 90 min to test the reliability and the blocking behavior of the devices was measured at 15 min intervals at room temperature.

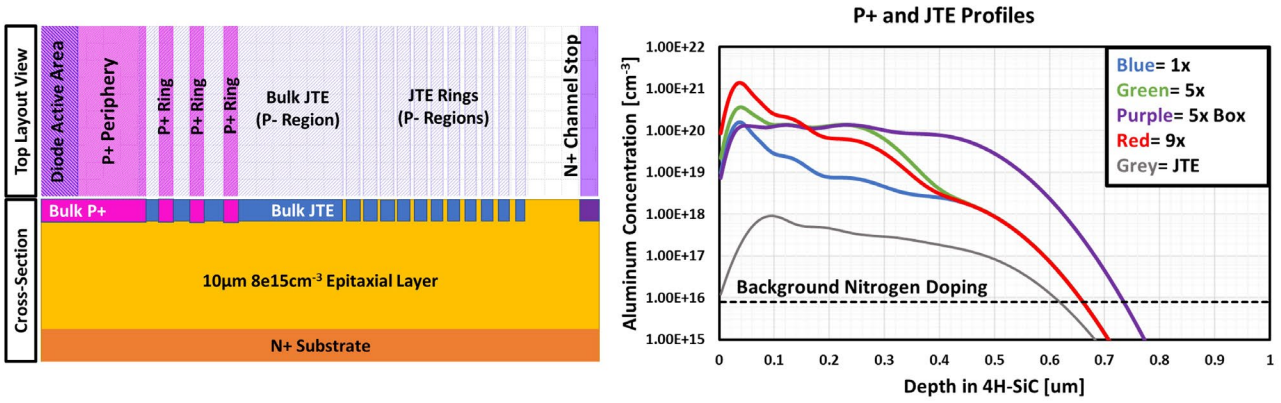

(a) (b)

Figure 1. (a) Cross-sectional and top view of one side of the PiN device structure. (b) Concentration profile of N doping level of epilayer, and implanted Al concentration profiles simulated by SRIM for PiN diodes, where 1×10^{15} cm^{-2}, 5×10^{15} cm^{-2}, 5×10^{15} cm^{-2} box profile and 9×10^{15} cm^{-2} are denoted as "1x", "5x", "5x Box" and "9x", respectively.

Synchrotron Monochromatic Beam X-ray Topography in Grazing Incident Geometry (SMBXT) is an X-ray imaging technique capable of revealing the structural defects in the crystal up to the X-ray penetration depth. Experimental setup for SMBXT is shown in Fig. 2. Monochromatic beam (E = 8.9 keV) is used in SMBXT and $11\bar{2}8$ grazing incident reflection is recorded on high resolution X-ray films. Experiments were carried out at Beamline 1-BM at the Advanced Photon Source (APS), Argonne National Laboratory.

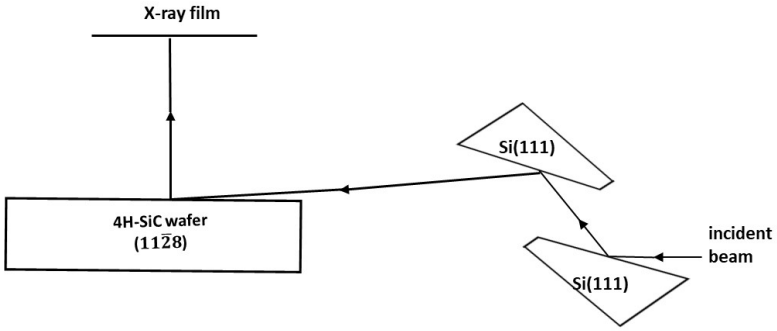

Figure 2. Schematic of the experimental setup for SMBXT.

Discussion

The $11\bar{2}8$ grazing incidence topographs of two sets of PiN diodes for each of the 6 implantation conditions are shown in Fig. 3. The topographs are characterized by a background microstructure of TSDs/TMDs (large white dot contrast), TEDs (small white dot contrast) and short BPD segments (black or white line contrast) most of which originate from the PVT-grown substrate and are replicated into the epilayer or in the case of BPDs mostly converted into TEDs. Each of these defects are highlighted in Fig. 3(a). Penetration depth of X-rays for the $11\bar{2}8$ reflection at 8.9 keV is estimated to be around 17 μm based on the method reported by Cheng and coworkers [14]. This depth is greater than the thickness of the epilayer indicating that the topographs contain contributions from the substrate as well. The topographs of 1xRT (Fig. 3(a)), 1xHT (Fig. 3(b)) and 5xHT (Fig. 3(d)) implanted PiN diodes do not show any BPDs generated due to implantation. On the other hand, topographs from devices fabricated with 5xRT (Fig. 3(c)), 5x Box RT (Fig. 3(e)) and 9xRT (Fig. 3(f)) show nucleation and motion of BPDs from the JTE regions, due to implantation and annealing process. These implanted induced BPDs are located near the edges of the active regions and show

similar configurations and are clearly different from those in the bulk substrate whose positions and line directions are more likely to be random.

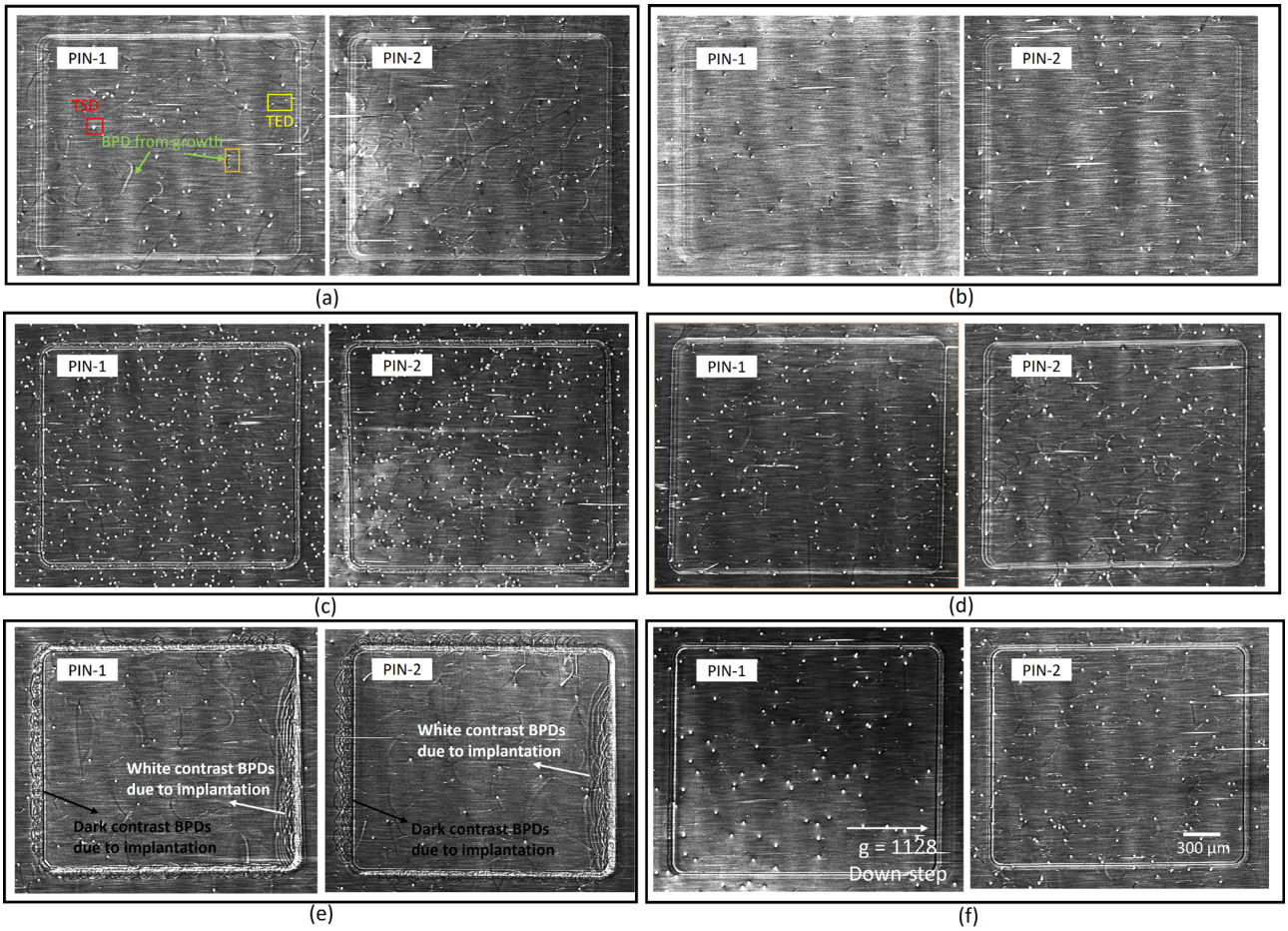

Figure 3. $11\bar{2}8$ synchrotron monochromatic beam X-ray topographs of two PIN diodes (PIN-1 and PIN-2) implanted under (a) 1xRT (TSD in red box, TED in yellow box, BPD in substrate converted to TED in epilayer in orange box) (b) 1xHT (c) 5xRT (d) 5xHT (e) 5x Box RT (f) 9xRT.

Fig. 4 shows enlarged images from some selected regions of the topographs in Fig. 1 with the P+ rings of the JTE regions highlighted in red boxes. Other than the contrast from the JTEs, no defect contrast is visible for P+ rings of the JTE regions of the 1xRT, 1xHT, and 5xHT implanted devices while contrasts from these regions are blurred by overlapping line contrasts likely from segments of BPDs in 5xRT, 5x Box RT and 9x RT devices. For the diodes implanted with 1x under both RT and HT, there is no evidence of dislocations generated due to implantation and annealing since the dosage is relatively low. However, the formation of BPD half loops, can be observed from the edge of the active device area or the P+ rings when the dose level is elevated to 5x and 9x. The BPD densities in the JTE regions of 5x RT device (Fig. 4(c)) appear to be slightly higher than those of 9x RT (Fig. 4(g)), since the extent of blurred contrast in the JTE region is wider on the topograph. The most extensive nucleation and motion of BPDs due to implantation and annealing is observed for the 5x Box RT (Fig. 4(e) and (f)). This suggests that the generation of BPDs due to implantation and annealing process is not merely determined by the dosages, but the implanted concentration profile may also play a role in the formation of BPDs. 9x RT has higher surface concentration and lower body concentration, while 5x RT and 5x Box RT have relatively low surface concentration and higher body concentration. To obtain a high body concentration profile, more high energy ions will penetrate the surface and generate more vacancies/interstitials that could increase the strain leading to higher density of BPDs. Note that Fig. 4(d) showing topographs of PiN diodes implanted with 5xHT do not contain BPDs in the JTE regions. This absence of BPDs in the HT implanted device compared to the

RT implanted device to the same concentration profile suggests the generation of BPDs is supressed by the high temperature condition through dynamic annealing.

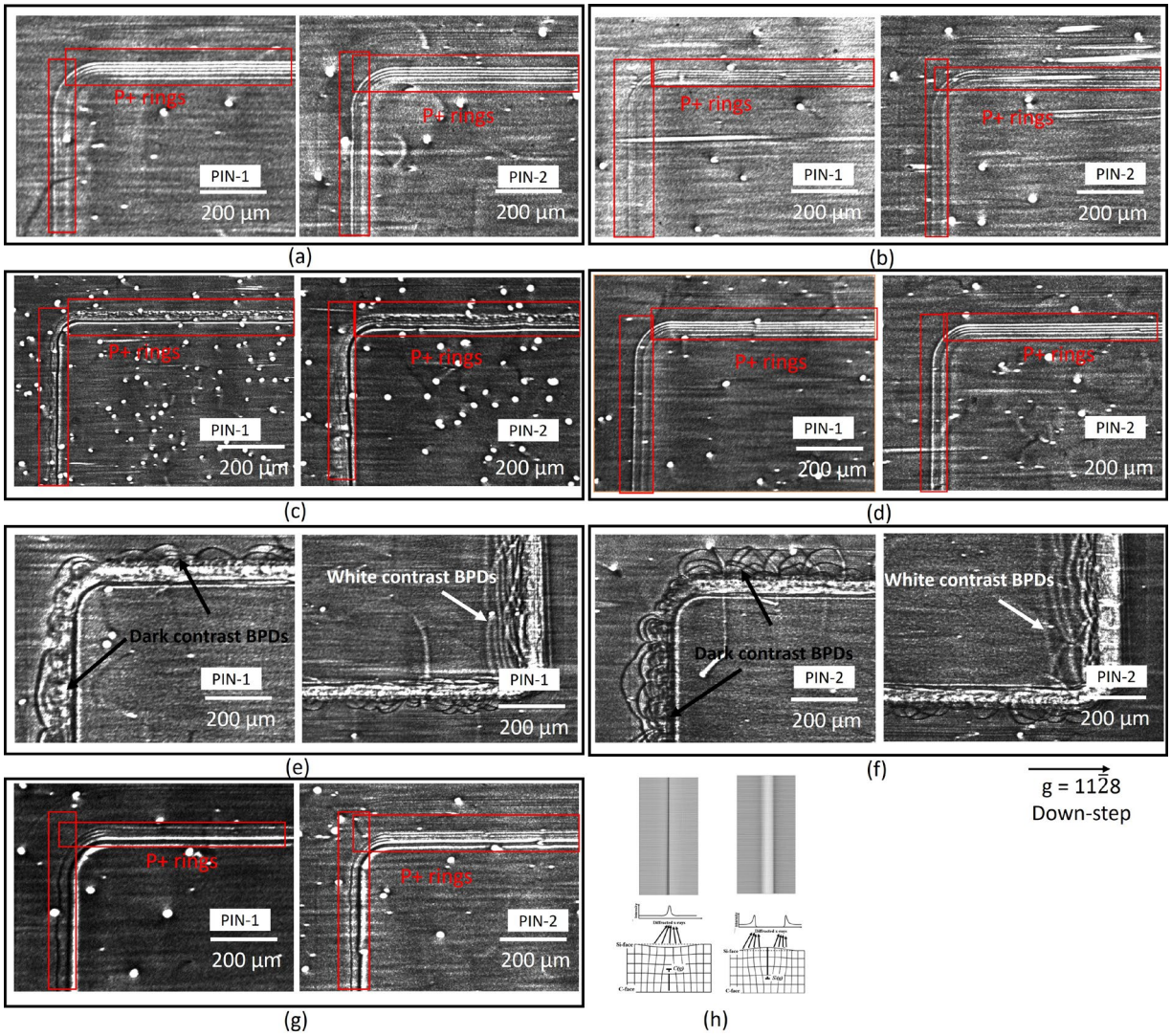

Figure 4. Enlarged $11\bar{2}8$ synchrotron monochromatic beam X-ray topographs of two PIN diodes (PIN-1 and PIN-2) implanted under (a) 1xRT (b) 1xHT (c) 5xRT (d) 5xHT (e) and (f) 5x Box RT (g) 9xRT; (h) ray tracing simulation of edge type BPD with extra half plane pointing up and down.

BPD half loops with black and white contrasts are indicated by arrows in enlarged topographs of devices implanted with 5x Box RT (Fig. 4(e) and (f)). The dark contrast BPDs tend to move away from the device, while the white BPDs move in the oppposite direction. Such BPD half loops are composed of edge and screw components, where segments of the half loops, with line directions of $[1\bar{1}00]$ and Burgers vectors of $\frac{1}{3}[11\bar{2}0]$, are edge components. Ray tracing simulations of the edge components of the BPD half loops located on the left and right sides of the devices, are shown in Fig. 4 (h). The simulated images that manifest dark BPDs have their extra half planes pointing down, while white BPDs have their extra half planes pointing up. After the implantation process, the implanted regions undergo three dimensional lattice expansion leading to tensile stress. During the annealing process, BPDs can be nucleated on the surface at the boundary between the P+ and P- region, since the implantation at different Al concentrations between the two regions can introduce lattice mismatch strains. Fig. 5 summarizes the behavior of BPDs at the two different boundaries bordering the device, illustrating the movement of dark BPDs on the left edge of the device, where P- region is located to the left of the P+ region. Compared to the P+ regions, the P- region has lower tensile stress after implantation. Therefore, this will induce the dark BPDs with extra half plane pointing down to glide into the P- region along the inclined basal plane. On the other side of the

device, where P- region is located at the right side of the device, the higher tensile stress of the P+ region will induce the movement of white BPD with extra half plane pointing up into the P+ region. While the mismatch stress between the P+ and P- regions are responsible for the initiation of glide of the two types of BPDs, the glide process continues beyond these regions into the unimplanted areas for black BPDs and active device areas for white BPDs. The largest width of the lateral expansion of white BPDs along $[11\bar{2}0]$ direction is measured to be 185 μm in PIN-1 corresponding to 13 μm of depth, greater than the 10 μm thickness of the epilayer. This indicates the white BPDs nucleated from the surface of the epilayer glide through the epilayer into the substrate. Since the white BPDs have extra half plane pointing up, they will not stop at the epi/sub interface to relax the misfit stress induced by difference of the lattice parameter due to different background doping levels of epilayer and substrate. However, in the case of the dark BPDs, they have extra half plane point down, which can relax the misfit stress resulting in the formation of interfacial dislocations at the epi/sub interface. The largest width of the lateral expansion of dark BPDs in PIN-1 is measured to be 114 μm corresponding to 8 μm of depth, indicating these are still restricted to be within the epilayer and have not contributed to relaxation. The formation and movement of these BPDs by the implantation and annealing processes can significantly impact the performance of the devices. Therefore, these processes must be optimized, such as the use of high implantation temperatures when the dose level is high or using different concentration profiles, to avoid process-induced BPDs.

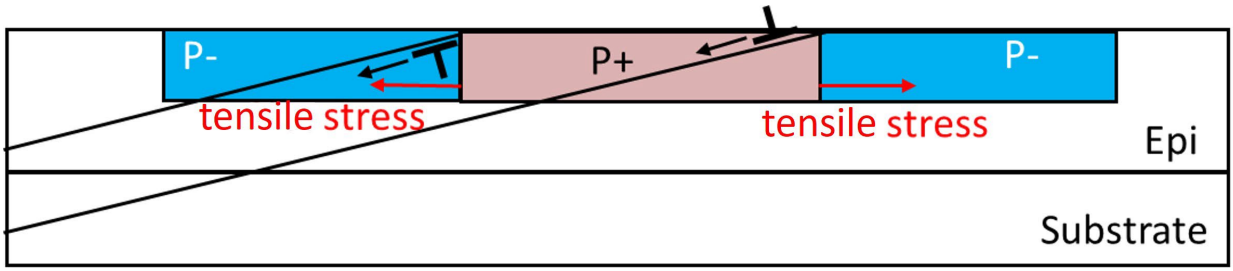

Figure 5. Schematic cross section of PIN diode showing movement of dark contrast BPDs with extra half plane pointing down and white contrast BPDs with extra half plane pointing up.

Numerous studies have shown that BPDs in the epilayer can undergo Shockley-type stacking fault (SSF) expansion during forward bias operation of PiN diodes, where the energy released by electron-hole recombination can drive the Si-core partial dislocation to glide leaving a SSF between the two partials [15, 16]. Zhao and coworkers have also reported that leakage currents correlate with the density of BPDs in the devices [17]. The blocking behavior of the 6 types of PiN diodes in this study measured before the current stress procedure revealed higher leakage currents for devices implanted with 5x Box RT and 5x RT [8], as shown in Fig. 6 and 7. Based on the distribution of the curves, the trend is not obvious for effect degradation of blocking voltage due to difference in dose. However, this result correlates with the density of process-induced BPDs observed on the X-ray topographs of such devices. Current stressing at 125 A/cm^2 for up to 90 min at room temperature for these 6 PiN diodes reveals that 1x RT/HT, 5x HT and 9x RT device suffer little degradation whereas 5x Box RT and 5x RT devices show severe increase in leakage currents. Moreover, the degradation of device implanted with 5x Box RT was too significant to complete the stressing procedure and the measurement was ceased at 30 min. Overall, a strong correlation can be made with the density of process-induced BPDs observed on the X-ray topographs of these devices. Studies are underway to examine the mechanism of leakage due to process-induced BPDs.

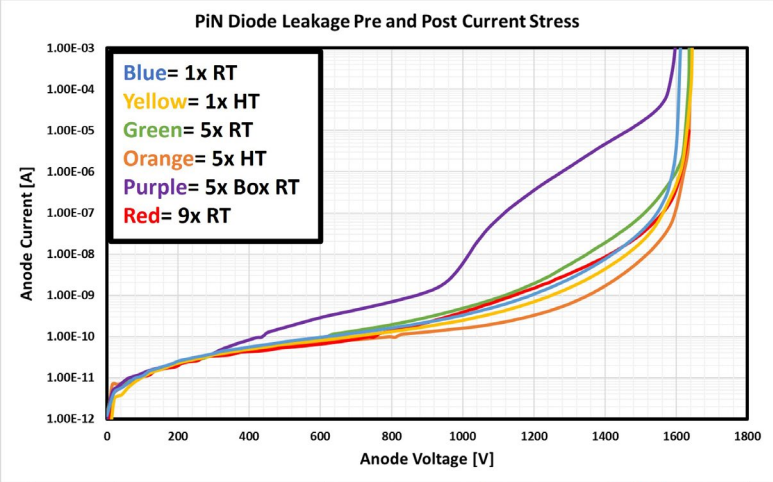

Figure 6. Blocking behavior of devices fabricated under different conditions

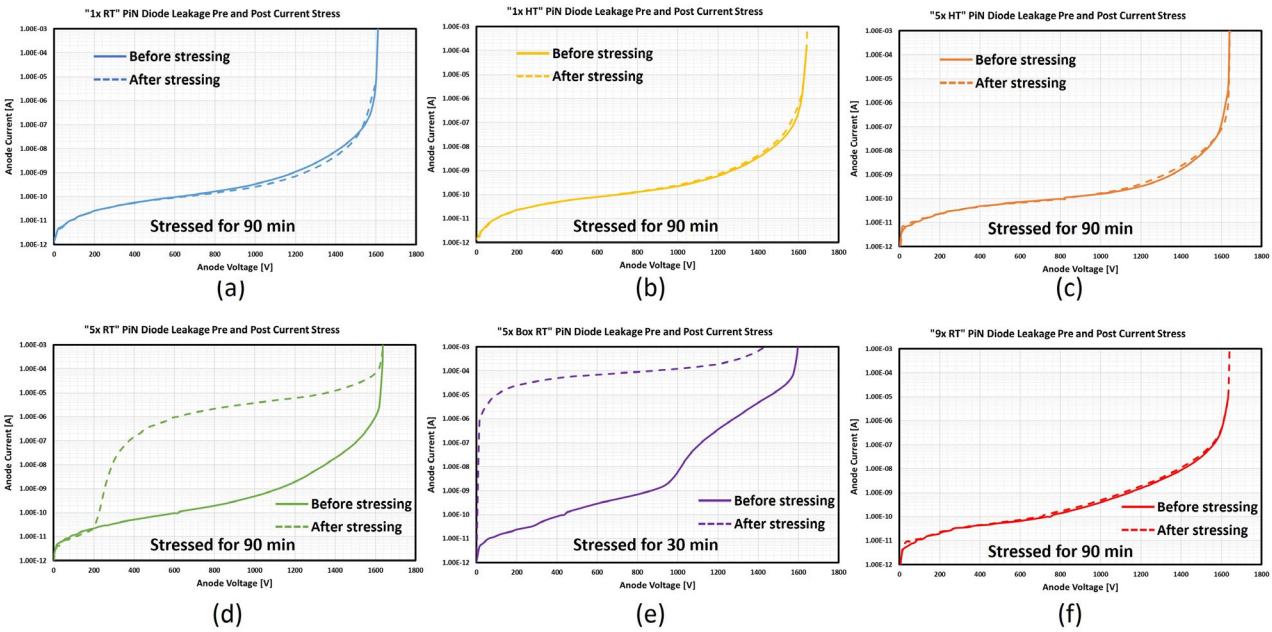

Figure 7. Blocking behavior of devices before and after applying current stress of (a) 1xRT (b) 1xHT (c) 5xHT (d) 5xRT (e) 5x Box RT (f) 9xRT

Summary

PIN diodes, fully fabricated on 4H-SiC wafer with 10 μm thick epilayer with different implantation conditions and the same annealing temperature, have been characterized by SMBXT to understand and comprehensively study the nature of the BPDs introduced by the implantation and annealing processes. It is found that formation of process-induced BPD is suppressed under implantation with relatively low dose level condition or relatively high dose level but at high temperatures. Moreover, the concentration profile of implantation can also affect the formation of BPDs, with more BPDs nucleated in devices with a box concentration profile. In addition to that, opposite sign process-induced BPDs migrate in opposite directions under the same implantation induced stress. The density of these BPDs correlates with higher leakage currents during current stressing measurements. Thus the formation and movement of these process-induced BPD can negatively impact the performance of the devices and all fabrication processes must be optimized to avoid that.

Acknowledgments

This research used resources of the Advanced Photon Source, a U.S. Department of Energy (DOE) Office of Science User Facility operated for the DOE Office of Science by Argonne National Laboratory under Contract No. DE-AC02-06CH11357. The Joint Photon Sciences Institute at SBU provided partial support for travel and subsistence for access to Advanced Photon Source.

References

[1] J. Guo, Y. Yang, B. Raghothamachar, T. Kim, M. Dudley, J. Kim, J. Cryst. Growth 480 (2017) 119-125.

[2] F. Roccaforte, P. Fiorenza, M. Vivona, G. Greco, F. Giannazzo, Materials 14(14) (2021) 3923.

[3] Z. Chen, H. Peng, Y. Liu, Q. Cheng, S. Hu, B. Raghothamachar, M. Dudley, R. Ghandi, S. Kennerly and P. Thieberger, Materials Science Forum 1062, 361-365

[4] Z. Chen, Y. Liu, H. Peng, T. Ailihumaer, Q. Cheng, S. Hu, B. Raghothamachar, M. Dudley, ECS Transactions 104, 75 (2021)

[5] K. Konishi, R. Fujita, Y. Mori and A. Shima, Semiconductor Science and Technology 2018 Vol. 33 Issue 12

[6] M. Nagano, H. Tsuchida, T. Suzuki T. Hatakeyama, J. Senzaki and K. Fukuda, J. Appl. Phys. 108, 013511 (2010)

[7] R. E. Stahlbush, N. A. Mahadik,. J. Zhang, A. A. Burk, B. A. Hull, J. Young, Mater. Sci. Forum, vols. 821-823, pp 387-390, June 2015.

[8] S. Mancini, S. Y. Jang, Z. Chen, D. Kim, Y. Liu, B. Raghothamachar, M. Kang, A. Agarwal, N. Mahadik, R. Stahlbush, M. Dudley, W. Sung, proceeding of 2022 IEEE International Reliability Physics Symposium (IRPS).

[9] J.García López, Y. Morilla, J.C. Cheang-Wong, G. Battistig, Z. Zolnai, J.L. Cantin, Nuclear Instruments and Methods in Physics Research Section B: Beam Interactions with Materials and Atoms, 267(7), 1097-1100.

[10] Y. Zhang, W. J. Weber, W. Jiang, C. M. Wang, and V. Shutthanandan, Journal of Applied Physics 95, 4012 (2004)

[11] B. Raghothamachar, M. Dudley, Vol. 10, ASM Handbook (2019 Edition), ASM international, 2019, p 459-477.

[12] T. Ailihumaer, H. Peng, Y. Liu, Q. Cheng, Z. Chen, S. Hu, B. Raghothamachar and M. Dudley, ECS Transactions 104 (7), 157

[13]The Stopping and Range of Ions in Matter (SRIM) in James Ziegler's SRIM-2008 program: http:// www.srim.org.

[14] Q. Cheng, H. Peng, S. Hu, Z. Chen, Y. Liu, B. Raghothamachar and M. Dudley, Materials Science Forum 1062, 366-370

[15] M. Skowronski and S. Ha, J. Appl. Phys., vol. 99, 011101, 2006.

[16] T. Kimoto, A. Iijima, H. Tsuchida, T. Miyazawa, T. Tawara, A. Otsuki, T. Kato and Y. Yonezawa, 2017 IEEE International Reliability Physics Symposium (IRPS), 2017, pp. 2A-1.1-2A-1.7, doi: 10.1109/IRPS.2017.7936253.

[17] F. Zhao, M. M. Islam, B. K. Daas and T. S. Sudarshan, Materials Science Forum, vol. 64, pp. 281–283, 2010, doi: 10.1016/j.matlet.2009.10.062.